RESEARCH ARTICLE

Numerical and Experimental Investigation of Thickness Effect on the Cambered Airfoils at Low Reynolds Numbers

Düşük Reynolds Sayılarında Kambur Kanat Profillerinde Kalınlık Etkisinin Sayısal ve Deneysel Olarak İncelenmesi

Muhammer Ayvazoğlu[1] , Sinem Keskin[1] , Rumeysa Şahin[1] , Mehmet Sincar[1] , Eren Anıl Sezer[1] , Halil Hakan Açıkel[1] , Mustafa Özden[2] , Mustafa Serdar Genç[1]*

[1] Wind Engineering and Aerodynamics Research Lab., Erciyes University, 38039, Kayseri, Türkiye.
[2] Energy Innovation Center, North Charleston, Clemson University, 29405, SC, USA.

Abstract

In this study, experimental and numerical study for the cambered airfoils was conducted at $Re = 1.5 \times 10^5$ and $Re = 2.5 \times 10^5$ and different angles of attack. In the experimental analysis, oil-flow visualization and force measurement techniques were utilized. For numerical analysis, the k-w SST transition model was used to predict the flow over the cambered airfoils. The time-dependent aerodynamic force coefficients of the cambered NACA2412, NACA2415 and NACA2418 airfoils pointed out the force fluctuations formations due to unsteady flow on the airfoils. Whereas the force coefficient increased as the airfoil thickness increased, a decrease in the lift coefficient was observed due to adverse pressure gradients. Moreover, as the airfoil thickness increased, the separation occurred earlier due to the effect of adverse pressure gradients, so it got closer to the leading edge and became shorter. However, the prediction of the separation point was delayed in numerical analysis and the prediction of the reattachment points was more consistent.

Keywords: Airfoil, lift coefficient, transition model, oil-flow visualization

Öz

Bu çalışmada, kambur kanat profilleri için $Re = 1.5 \times 10^5$ ve $Re = 1.5 \times 10^5$ ve farklı hücum açılarında deneysel ve sayısal çalışmalar yapılmıştır. Deneysel analizde, yağ akışı görselleştirmesi ve kuvvet ölçüm teknikleri kullanılmıştır. Sayısal analiz için ise, bu kambur kanat profilleri üzerindeki akışı tahmin etmek için k-w SST türbülansa geçiş modeli kullanılmıştır. Kambur NACA2412, NACA2415 ve NACA2418 kanat profillerinin zamana bağlı aerodinamik kuvvet katsayıları, kanat profilleri üzerindeki kararsız akış nedeniyle kuvvet dalgalanmalarının oluştuğunu göstermiştir. Kanat profili kalınlığı arttıkça kuvvet katsayısı artarken, ters basınç gradyanlarından dolayı kaldırma katsayısında azalma gözlenmiştir. Ayrıca kanat kalınlığı arttıkça ters basınç gradyanlarının etkisiyle ayrılma daha erken meydana gelmiş, dolayısıyla hücum kenarına yaklaşmış ve kısalmıştır. Bunların yanında, sayısal analizde ise ayrılma noktasının tahmini gecikmiş ve yeniden bağlanma noktalarının tahmini daha tutarlı olmuştur.

Anahtar Kelimeler: Kanat profili, taşıma katsayısı, türbülansa geçiş modeli, yağ ile akış görselleştirme

1. INTRODUCTION

Today, it is one of the main requirements to consider aerodynamics-related issues in the design process of spacecraft, unmanned air vehicle, aircraft and wind turbines. An

important classification of those to investigate the aerodynamic performance is determining the operation flow regime. The field of low Reynolds aerodynamics has reached a highly-demand position since advances in aeronautics, energy industry, and especially the unmanned air vehicles [1]. This regime is generally defined for flows with Reynolds numbers smaller than 5×10^5 [2]. At low Re flows, viscous forces are likely to be more dominant compared with the inertial forces. As a result of this dominancy, the development of different flow characteristics can be observed. Boundary layer formation is one of the key issues while examining the flow over a surface since the aerodynamic performance of a plate or an airfoil is strongly influenced by this phenomenon.

As the fluid moves through the leading edge of an airfoil or surface, due to the no-slip condition caused by the viscous properties of the surface and the fluid, fluid molecules near the surface are forced not to slip and upstream molecules are also affected by those because of intermolecular forces. At Reynolds numbers lower than 5×10^5, disturbances, those can be assumed to be as a trigger for laminar to turbulent transition, are resisted by the laminar boundary layer [1][1]. As a consequence of this laminar boundary layer formation, flow separates from the surface under the influence of adverse pressure gradients, forming laminar separation bubble (LSB).

Another concept being investigated by aerodynamic researchers is called shear layer. It is a layer consisting of concentrated vortices those have a strictly varying tangential component of velocity [3]. After the flow separates from the surface, a transition region to turbulence is observed. Following this behavior, flow begins to reattach to the surface with the momentum transferred from the free stream primarily as the shear layer [4]. After reattachment of the flow, a later separation is generally not observed near trailing edge as a result of energy gain from free stream and flow has tended to be attached to the surface. As the reattachment occurs, a LSB formation happens. The position and length of the LSB are influenced by various factors such as turbulence intensity in freestream, Reynolds number, attack angle, etc. [5]. Both flow separation and formation of LSB cause a disruption and reduction in lift coefficient and rise in drag, besides, the closer LSB presence is to the leading edge, the earlier the lift curve recovers [6].

There are several experimental and numerical methods previously to identify the location of separation and LSB. Açıkel et al [7] performed a flow visualization technique, in which a wire with high resistance capacity is used, to obtain a clearly observable LSB formation. Additionally, a more advanced experimental method including measurement of velocity by hot-wire anemometry technique which is quite precise while examining the flow characteristics near the wall including boundary layer formation, flow separation, LSB presence, and turbulence intensity in freestream was conducted by Genç et al [8-17]. Another method is oil flow visualization in which an oil mixture was used to mark the separation and reattachment positions, but it is significant to make sure that it is sensible to flow quite enough to characterize the boundary layer [18].

Moreover, pressure-measurement based experimental methods provide additional inspects for defining the LSB behavior and transition region. Genç et al [13] performed pressure experiments controlled via a software on NACA2415 airfoil in a wind tunnel and considered C_p graphs in which stability on the curve proves that there is no pressure difference along the surface which means flow separates. There are also time-dependent force measurement experiments, those specify the stall conditions and locations, conducted at different Reynolds numbers and angles of attack. Genç et al [14] also determined the acoustic excitation effects on stall conditions for NACA2415. Koca et al [15] investigated the effect of local flexible membrane on different aerodynamic performance criteria over an airfoil and examined the LSB presence and different stall conditions.

Conducting a proper numerical technique to analyze the LSB formation requires an accurate solution which again requires a proper selection of turbulence model. Mainly based on the study performed by Emmons [19], Dhawan et al. made an experiment sourced correlation of intermittency which is again developed later by Steelant and Dick [20] by modelling a coupled formulation of Navier-Stokes and intermittency transport equation. Suzen at al [21] modified this formulation which will be able to solve the cross-stream flow in transition region. An effective solution of transition region with numerical methods is important to characterize and recognize the LSB formation. Menter et al. [22] integrated and calibrated the previous correlations by applying additional expressions those are able to control the size of LSB and coupling with the k-w SST model. The basic idea behind this transition model is to use the start point of the intermittency fluctuation which gives a background to correctly predict the LSB formation and transition behavior. Therefore, some momentum related quantities were used such as transition onset momentum thickness Reynolds number, and critical momentum thickness Reynolds number [22]. Including those in the equations provides a better predicting of nonlocal influences which are important to understand the transition region since the prediction of transition is strongly dependent on the freestream turbulence as well as laminar boundary layer. Since transition prediction in the low Reynolds flow regime is numerically difficult, research is still needed on this subject for more robust and accurate results.

1.1. Aim and Objective

In this study, the effect of airfoil thickness on the aerodynamic characteristics of NACA2412, NACA2415, and NACA2418 cambered airfoils, which are frequently used in aviation and wind energy applications, at low Reynolds numbers (Re $= 1.5 \times 10^5$ and Re $= 2.5 \times 10^5$) was examined. In this context, time-dependent lift force measurement was performed to analyze flow-induced fluctuations and stability. The separation, transition and reattachment regions were assessed by employing pressure measurement. The oil flow visualization technique was employed to grasp the structure and placement of the LSB. On the other hand, the numerical analyses were carried out utilizing the Menter's SST Transition model, therefore, the x-component skin friction coefficient and pressure

coefficient values were presented, and they were compared with the experimental results.

2. METHODOLOGY

Experimental set-up, measurements and visualization techniques, numerical approach and mesh independence study were considered in the subheadings of the methodology section.

2.1. Experimental Set-up

A series of experimental operations were completed with the objective of insight into the flow occurrence, and the relationship between airfoil thickness, and the LSB region on the upper surface of the airfoils.
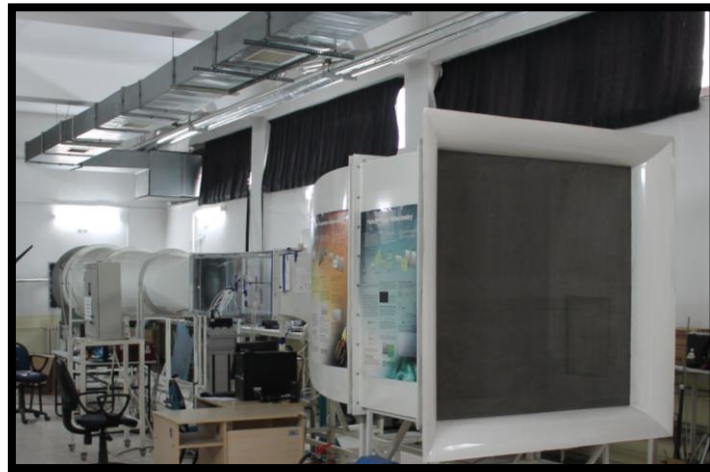
Figure 1. The perspective of the wind tunnel and the testing apparatus

The experimental investigations were carried out in a low-speed, suction-style wind tunnel including a plexiglass test section measuring 50 cm by 50 cm in Erciyes University, as shown in Figure 1. In the tunnel's operating area, the turbulence intensity is 0.9% at the smallest flow velocity and 0.3% at the maximum flow velocity [13].
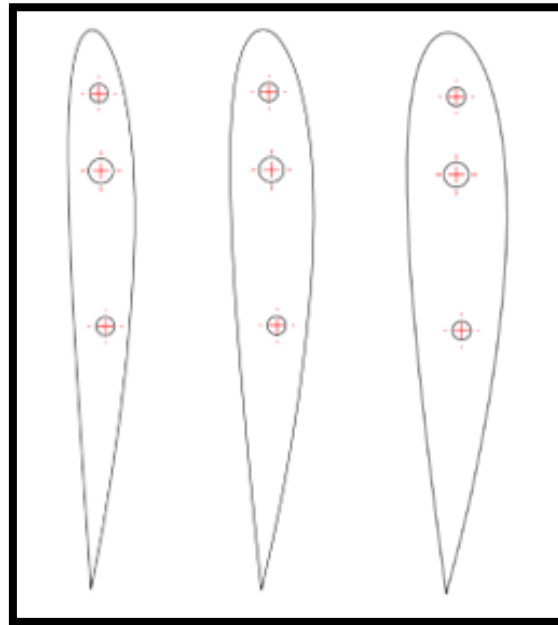
Figure 2. The sectional view of cambered airfoil specimens, NACA2412, NACA2415, NACA2418 respectively.

Airfoils with rigid and pressure tap were designed in SolidWorks software as seen in Figure 2. and Figure 3. Afterwards, they were produced with the help of 3D printer. The produced prototypes were sprayed with matte black dye after being sanded to eliminate any surface imperfections. At either end of the airfoils, rectangle transparent endplates were used to hinder the intervention of tip vortices. The technical parameters for the airfoils suggested are shown in Table 1.
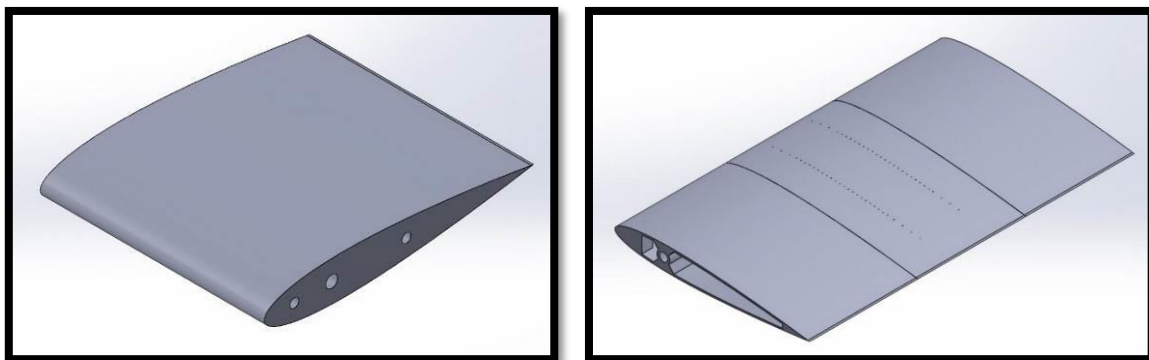
Figure 3. The rigid and pressure tap designed airfoils.

Table 2. Technical definition of considered airfoils.

Parameter	Definition
Airfoil	NACA2412
	NACA2415
	NACA2418

Chord length (m)	0.18
Span length (m)	0.30
Max. camber and its location (%)	2 and 40

2.1.1. Aerodynamic Force Measurement

The aerodynamic force measurement was performed to gauge time-dependent lift forces (F_L). The initial components of the system were a data converter and load cells to measure the aerodynamic forces, as shown in Figure 4. Before the experiment, the load cells were exposed to specific loads to perform the calibration operation. In terms of data collecting, a 10-second sample rate of 1 kHz was employed. The lift coefficient (C_L) was calculated from the reported lift forces utilizing following equation:

$$C_L = 2F_L / \rho U_\infty^2 A \qquad (1)$$

where FL is lift force, ρ is density of fluid, U∞ is freestream velocity and A is surface area.
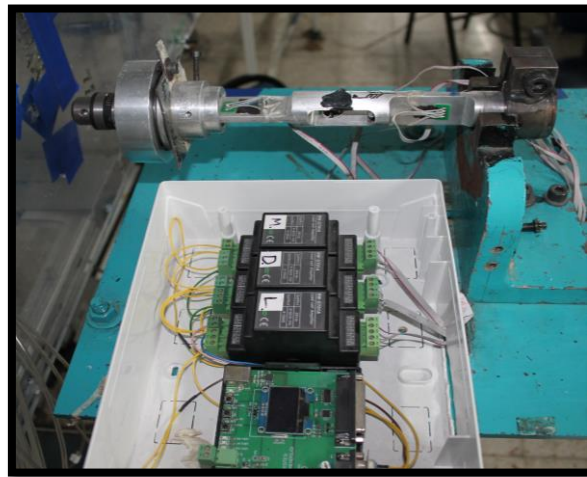
Figure 4. The view of strain-gauge components for aerodynamic force measurement.

2.1.2. Pressure Measurement

Fifty-one pressure taps with a diameter of 0.8 mm are positioned in a double row of twenty-eight along the chord in the middle part of the airfoils, and twenty-three in a single row at the bottom of the airfoils as indicated in Figure 5. A diaphragm -type pressure transducer (Figure 5.) was used to measure the pressure distributions on the suction and pressure surface of airfoils, and obtained data were coupled with a signal converter. The pressure difference obtained from each pressure tap and the pressure coefficient (C_p) are provided as following equation:

$$C_P = 0.5(p - p_0) / \rho U_\infty^2 \qquad (2)$$

where, p is the static pressure at each considered point, p_0 is the stagnation pressure of the freestream in the wind tunnel.

Figure 5. The sample of pressure test airfoil and diaphragm-type transducers.

2.1.3. Oil Flow Visualization

An oil flow visualization procedure was applied to observe flow-field on the airfoils. The oil flow visualization apparatus was created. The oil flow visualization apparatus was designed on the basis of preparing an oil mixture (Figure 6) and covering the airfoil's upper surface with this mixture using a soft bristle brush.
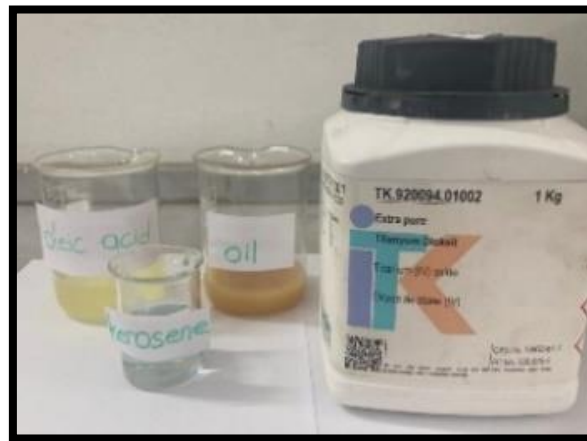
Figure 6. The mixture component for oil flow visualization.

2.2. Numerical Approach

In terms of 2D numerical analysis, Reynolds-Averaged Navier–Stokes equations and the four-equation transition Shear Stress Transport (SST) turbulence model [23] was integrated, utilizing an academic-based Ansys FLUENT software to simulate the flow over the cambered airfoils. This turbulence model was adopted since it enables

acceptable outcomes concerning the accuracy of experimentation and clarifies the estimation of transition and LSB [24].
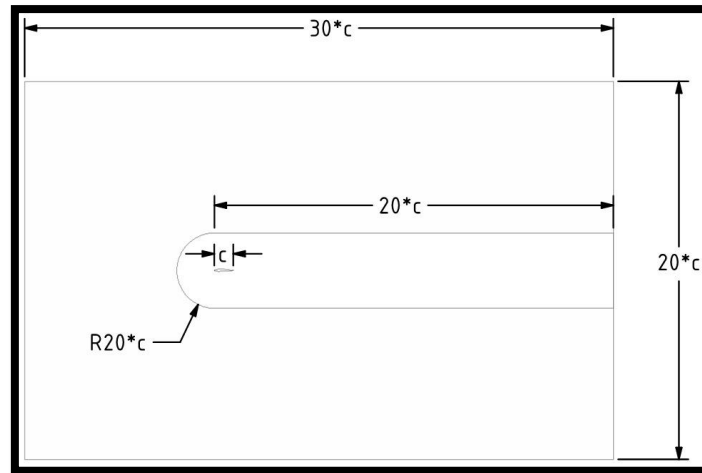
Figure 7. Sketch of domain and airfoil.

The computational domain was created (Figure 7.), and then a C-type and a hybrid unstructured grid was generated as depicted in Figure 8. A boundary layer mesh with normal growth ratio of 1.2 was applied to capture flow phenomena around the critical region for this study. The domain size was determined considering the airfoil's diameter. The airfoil is situated as the distance of its leading edge to the inlet is 10c and the distance to the outlet is 20c as shown in Figure 7. U_∞ =2.684 m/s and 4.473 m/s were at the inlet, constant pressure was at the outlet, and non-slip condition was on the airfoils. Table 2. presents comprehensive details regarding the computational mesh information that was provided.

Table 2. Principal features of numerical analysis.

Feature	Value
Airfoil	NACA2412 NACA2415 NACA2418
Chord length	1 m
Flow velocity	2.684 m/s - 4.473 m/s
First layer spacing	4×10^{-6} m
y+	<1
Far-field distance	30 m
Node numbers	$3.5x10^6$
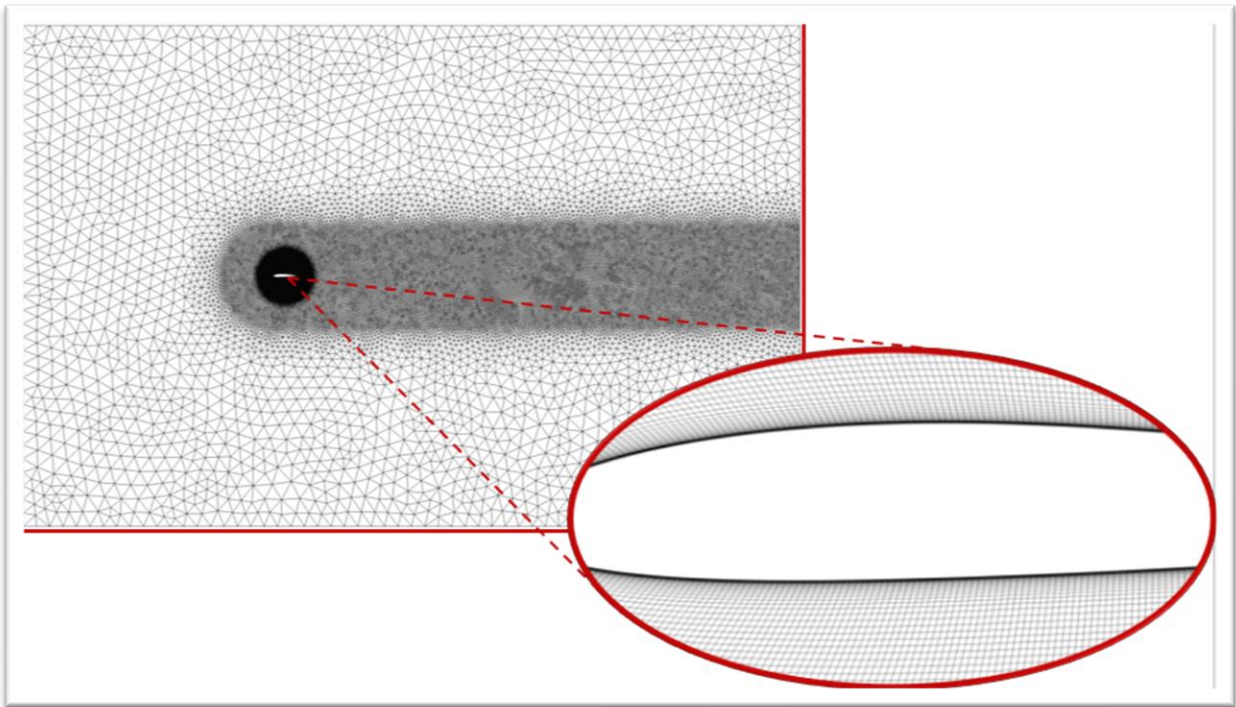
Figure 8. Mesh structure in the entire domain and boundary layer mesh around the airfoil.

2.2.1 Mesh independency study

To check computational analysis, a mesh independency study was performed. The analysis was conducted for the NACA2412 airfoil at Re=1.5×10^5 and AoA= 4°. Table 2. presents C_L and C_D values change according to the number of meshes. After the mesh size of 1.75×10^5, both aerodynamic coefficients remained constant. Since the reliability of the numerical study was ensured, the studies in the following sections were carried out with a mesh size of 3.5×10^5.

Table 2. Mesh independency results for NACA2412 at Re=1.5×10^5 and AoA= 4°.

Mesh Size	C_L	C_D
0.75×10^5	0.61	0.015
1.75×10^5	0.62	0.014
3.5×10^5	0.62	0.014
0.8×10^6	0.62	0.014
0.1×10^7	0.62	0.014

3. IMPLEMENTATION AND RESULTS

A series of experimental and numerical studies were carried out to examine the flow characteristics of three NACA series airfoil models with different thicknesses by emphasizing the LSB. Time-dependent force measurements were carried out at Re=1.5×10^5 and Re=2.5×10^5 at angles of attack of $0° < \alpha < 18°$. Particularly, the 13° of

angle of attack that is around the stall is highlighted in terms of CL. Pressure measurements were carried out for Re=1.5×10^5 and $\alpha = 4°$ and these results are presented in comparison with numerical findings for each airfoils. As another computational outcome, the plots of x- component skin friction were offered. The oil flow visualization experiment from the authors' previous study [18] is also provided for comparison purposes.

The graphs of the time-dependent aerodynamic force coefficients of the cambered NACA2412, NACA2415 and NACA2418 airfoils were given in Figure 9. These graphs were obtained from force measurements with the help of the automatic angle change system in our laboratory, the force value jumped with the angle changing, and then the time-dependent force change was recorded with 1000 samples per second for 10 seconds. When these graphs are examined, at Re = 1.5×10^5 (Figure 9a) it was seen that the force fluctuation was almost constant over time at lower angles of attack, and fluctuations in force results occurred due to unsteady flow on the airfoil as the angle increased. As shown in Figure 10, at Re = 1.5×10^5, the unsteady flow at an angle of attack of 13° around the stall angle and the oscillations in the lift force caused by changes in this flow over time are visible. At the post-stall condition, the increase in fluctuations due to the separated flow became very evident. In addition, while the force coefficient was expected to increase as the airfoil thickness increased, a decrease in the lift coefficient was observed along with an increase in the stall angle of the NACA2418 airfoil with 18%c thickness. This situation caused adverse pressure gradients to increase with increasing thickness in the cambered airfoil and the flow's inability to resist the viscous forces that dominate in flows at low Re numbers. At Re=2.5×10^5 (Figure 9b), with the increase in inertial forces, the flow on the airfoil became more stable and force oscillations decreased.
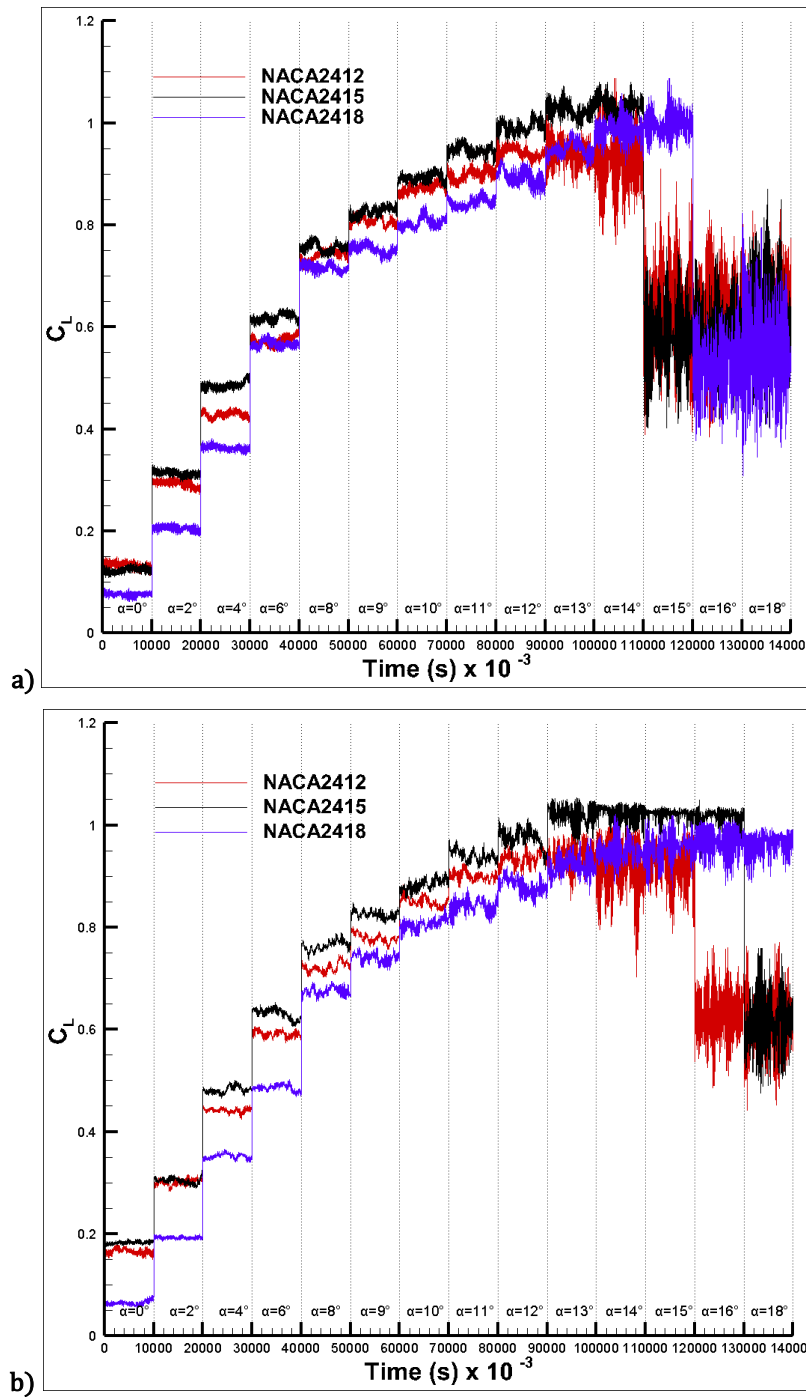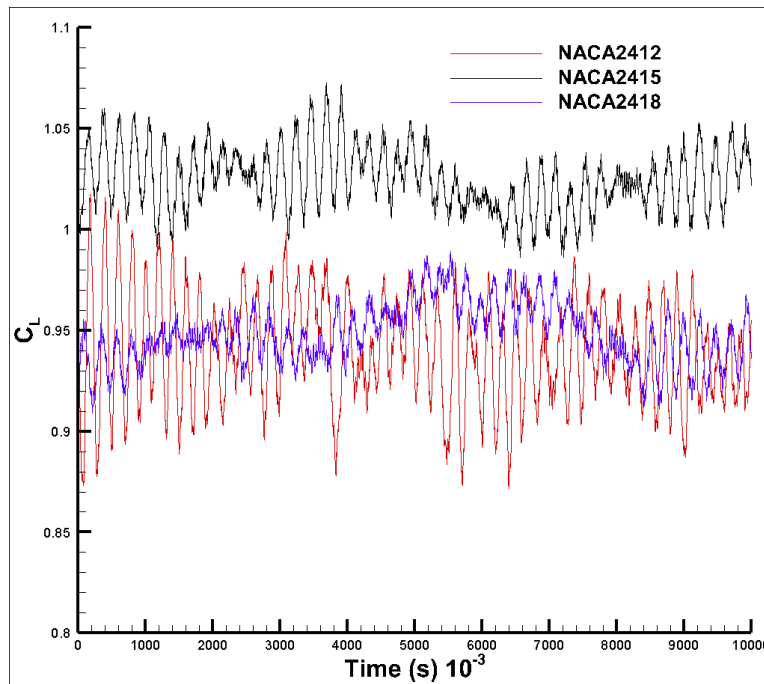
Figure 9. Time-dependent lift coefficient for NACA2412, NACA2415 and NACA2418 at a) Re = 1.5×10^5, b) Re= Re = 2.5×10^5.
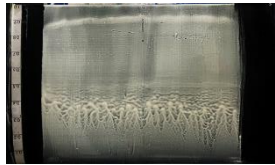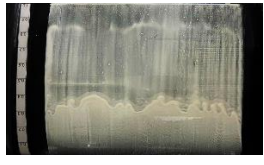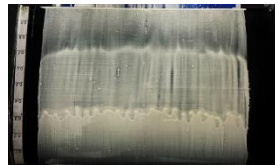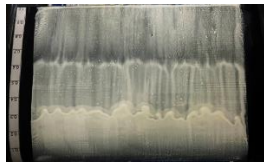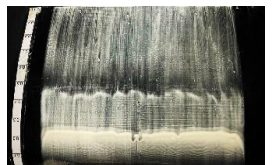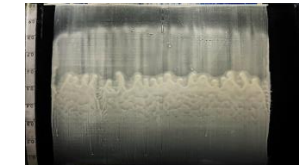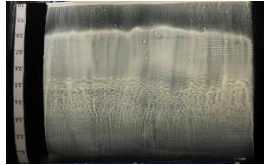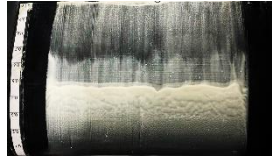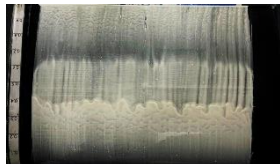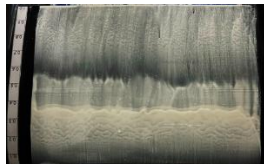
Figure 10. Variation of lift coefficients for the airfoils at Re $= 1.5 \times 10^5$ and $\alpha = 13$.

At Re$=1.5 \times 10^5$, the formation of separation bubbles due to viscous forces and adverse pressure gradients on the airfoil formed due to these bubbles and the small vortices caused fluctuations in the change of the force coefficient over time. The graphs showing the formation of these separation bubbles were shown in the oil flow visualization test results in Figure 11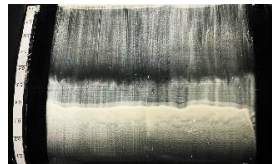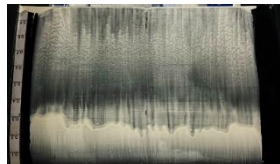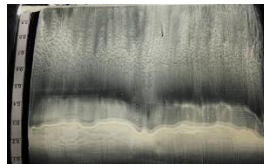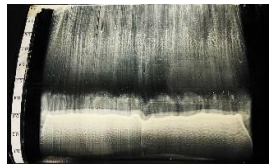, showing the formation of separation bubbles at different angles of attack and different Re numbers. At the same time, Figure 12 shows the separation and reattachment points in the flow in the x-component- skin friction (C_{fx})distributions obtained numerical results. The oil flow visualization results in Figure 11 showed that as the angle of attack increased, the separation bubble shrunk and moved towards the leading edge of the airfoil, also at the same angle of attack the bubble shrunk with the increase in inertia force. Additionally, as the airfoil thickness increased, the separation occurred earlier due to the effect of adverse pressure gradients, so it got closer to the leading edge and became shorter.

When the numerical analysis results obtained using the transition model in Figure 12 were compared with the oil flow experiment results in Figure 11, for example, for NACA2412, at Re $= 1.5 \times 10^5$ and AoA$=0°$, in the experiments the separation at x/c $= 0.38$ and the re-attachment at x/c $= 0.9$ occurred, and the bubble length was about 0.52c. In the numerical result, the separation occurred at x/c$=0.62$, reattachment at x/c$=0.86$, and the bubble length was 0.24c. As another example, for NACA2418, at Re$=1.5 \times 10^5$ and AoA$=4°$, the separation occurred at x/c$=0.25$ and the reattachment at x/c$=0.57$, while in numerical analysis, the separation was at x/c$=0.35$ and the reattachment was at x/c$=0.55$. This situation was shown from the pressure coefficient distribution results in Figure 13. When the results were evaluated, the prediction of the separation point was delayed in numerical analysis and the prediction of the

127

reattachment points was more consistent. Therefore, in the numerical analysis, the k-w SST transition model cannot yet make more accurate predictions for the flows at low Re numbers, and new detailed empirical equations being obtained from experimental results need to be added to this correlation-based model.

Re	AoA	NACA2412	NACA2415	NACA2418
1.5×10^5	0°			
	4°			
	8°			
2.5×10^5	0°			
	4°			
	8°			

Figure 11. Oil flow visualization results for the airfoils at Re=1.5×10^5 and Re=2.5×10^5 [18].

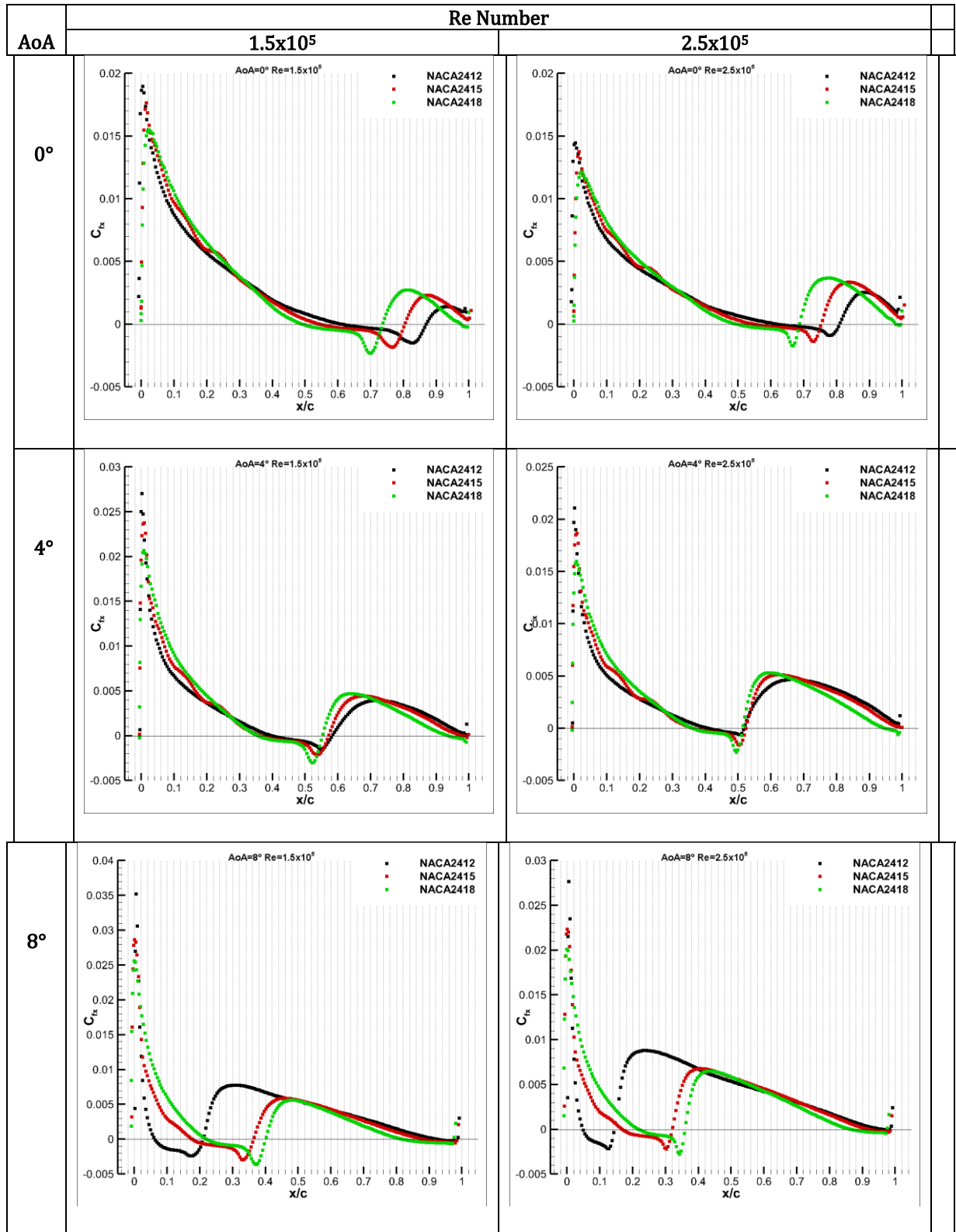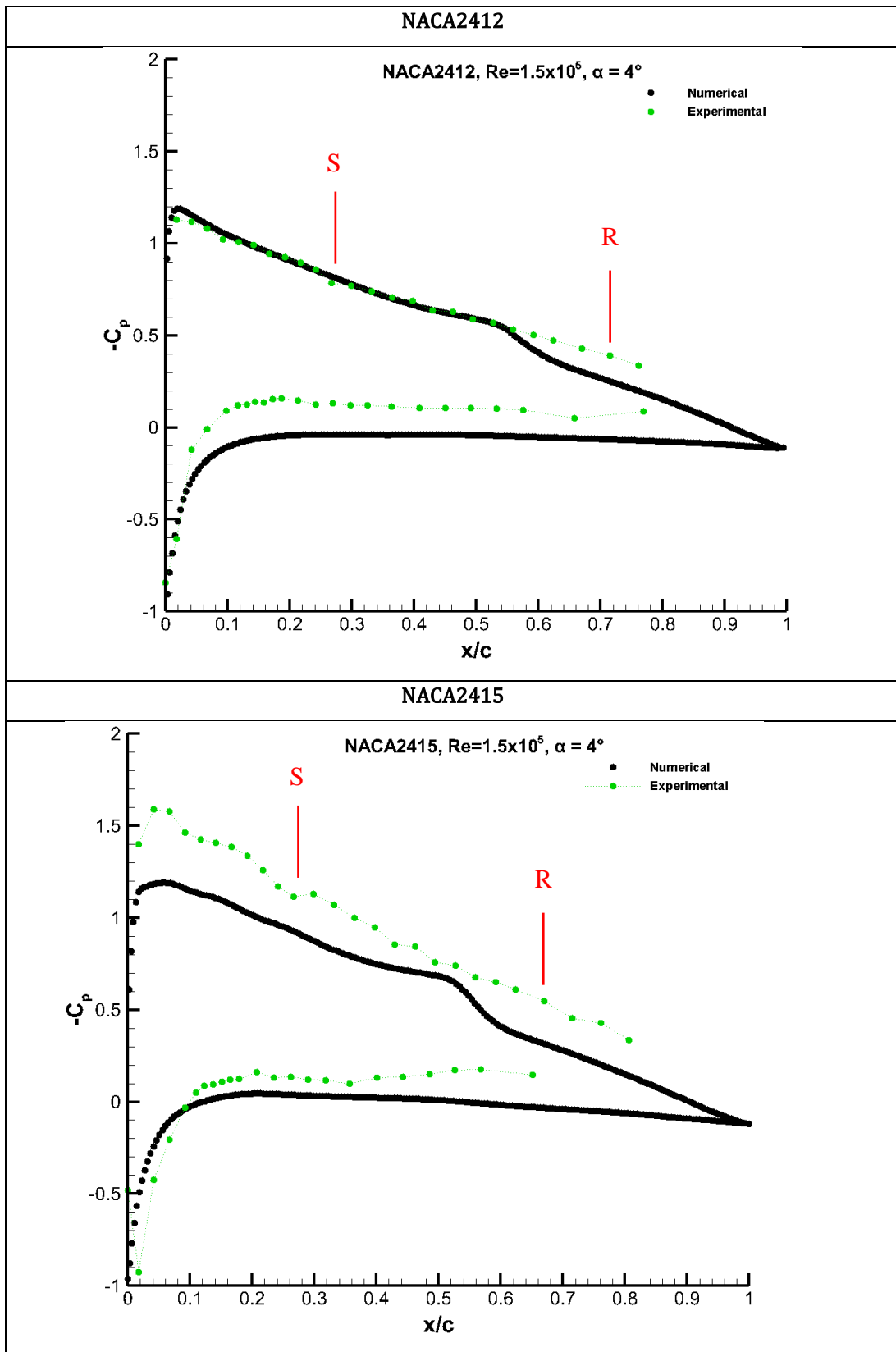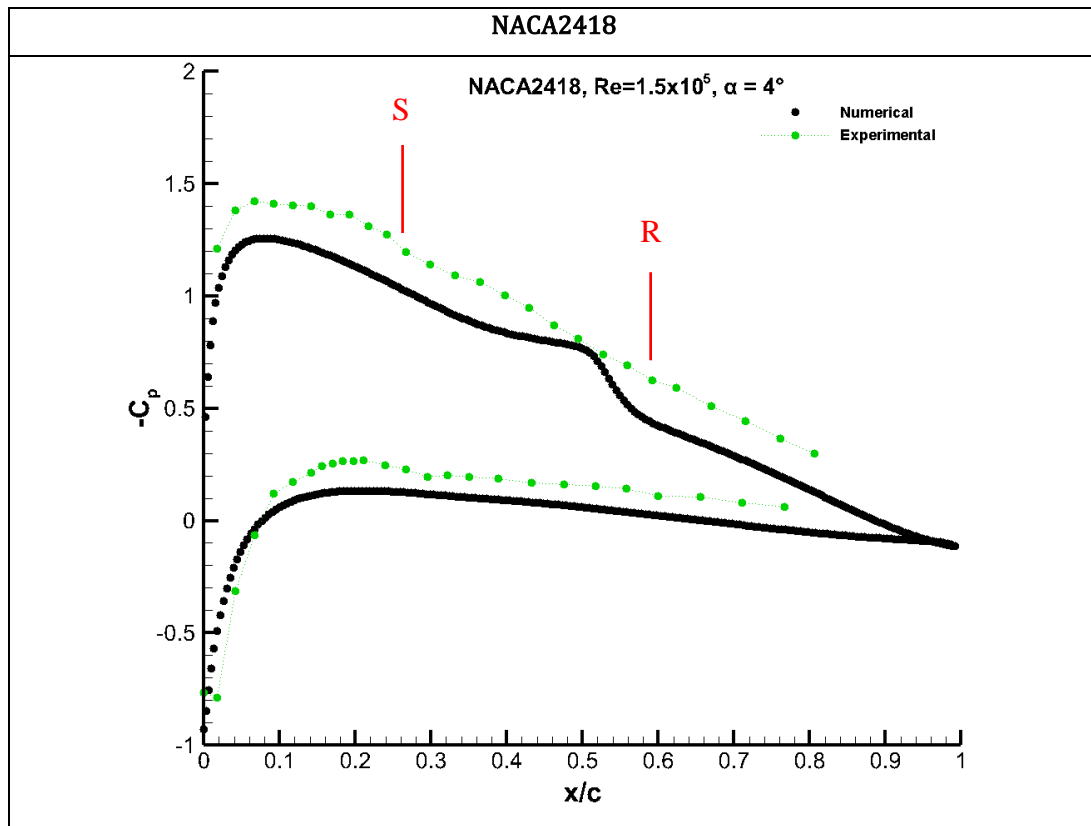**Figure 12.** Numerical C_{fx} results for cambered airfoils at Re=1.5x10^5 and Re=2.5x10^5.

Figure 13. The pressure coefficient distributions over the airfoils at Re = 1.5x10⁵ and α = 4°.

4. CONCLUSION

The time-dependent aerodynamic force coefficients of the cambered NACA2412, NACA2415 and NACA2418 airfoils showed that the force fluctuation was almost constant over time at lower angles of attack, and force fluctuations formed due to unsteady flow on the airfoils as the angle increased. At the post-stall condition, the increase in fluctuations due to the separated flow became very evident. Furthermore, while the force coefficient increased as the airfoil thickness increased, a decrease in the lift coefficient was observed due to adverse pressure gradients increasing and the flow's inability to resist the viscous forces at low Re numbers. The separation bubbles on the airfoil occurred and the small vortices due to the bubbles caused fluctuations in the change of the force coefficient over time. The oil flow visualization results showed that as the angle of attack increased, the separation bubble shrunk and moved towards the leading edge of the airfoil, also at the same angle of attack the bubble shrunk with the increase in inertia force. Additionally, as the airfoil thickness increased, the separation occurred earlier due to the effect of adverse pressure gradients, so it got closer to the leading edge and became shorter.

However, when the numerical and experimental results were evaluated, the prediction of the separation point was delayed in numerical analysis and the prediction of the reattachment points was more consistent. Therefore, in the numerical analysis, the k-w

131

SST transition model cannot yet make more accurate predictions for the flows at low Re numbers, and new detailed empirical equations being obtained from experimental results need to be added to this correlation-based model.

ACKNOWLEDGEMENT

REFERENCES

[1] L. W. Traub, C. Coffman, *Efficient Low-Reynolds-Number Airfoils*, Journal of Aircraft, **56**(2), 1-17 (2018).

[2] P. B. S. Lissaman*, Low-Reynolds-Number Airfoils,* Annual Review of Fluid Mechanics, **15**(1), 223–239 (1983).

[3] R. Krasny, M. Nitsche, *The onset of chaos in vortex sheet flow,* Journal of Fluid Mechanics, **454**, 47-69 (2002).

[4] J. Winslow., H. Otsuka, B. Govindarajan, I. Chopra, *Basic understanding of airfoil characteristics at low Reynolds numbers ($10^4 – 10^5$),* Journal of aircraft, **55**(3), 1050-1061, (2018).

[5] E.J. Fitzgerald, T. J. Mueller, *Measurements in a separation bubble on an airfoil using laser velocimetry,* AIAA journal, **28**(4), 584-592 (1990).

[6] Y. Patel, P. J. Ansell, "Airfoil Performance Sensitivity to Laminar Separation Bubble Topology," in *AIAA AVIATION 2023 Forum, San Diego, CA, USA, June 12-16, 2023,* pp. 3245.

[7] H.H. Açıkel, M.S. Genç, *Flow control with perpendicular acoustic forcing on NACA 2415 aerofoil at low Reynolds numbers,* Proceedings of the Institution of Mechanical Engineers, Part G: Journal of Aerospace Engineering, **230**(13), 2447-2462 (2016).

[8] M.S. Genç, *Control of low Reynolds number flow over aerofoils and investigation of aerodynamic performance,* Kayseri, (2009).

[9] K. Koca, M.S. Genç., H.H. Açıkel, M. Çağdaş, T.M. Bodur, *Identification of flow phenomena over NACA 4412 wind turbine airfoil at low Reynolds numbers and role of laminar separation bubble on flow evolution,* Energy, **144**, 750-764, (2018).

[10]   M.S. Genç, G. Özışık, N. Kahraman*, Investigation of Aerodynamics Performance of NACA0012 Aerofoil with Plain Flap,* Journal of Thermal Science and Technology, **28** (1), 1-8, 2008.

[11]   H.H. Açıkel, M.S. Genç, *Control of Laminar Separation Bubble over Wind Turbine Airfoil Using Partial Flexibility on Suction Surface,* Energy, **165**, 176-190, (2018).

[12]   K.S. Özden, İ. Karasu, M.S. Genç, *Experimental investigation of the ground effect on a wing without/with trailing edge flap,* Fluid Dynamic Research, **52**, 1–20, (2020)*.*

[13] M.S. Genç, İ. Karasu, H.H. Açıkel, *An experimental study on aerodynamics of NACA2415 aerofoil at low Re numbers,* Experimental Thermal and Fluid Science, **39**, 252-264, (2012).

[14] M.S. Genç, H.H. Açıkel, M.T. Akpolat, G. Özkan, İ. Karasu, *Acoustic control of flow over NACA 2415 aerofoil at low Reynolds numbers,* Sustainable Aviation: Energy and Environmental Issues, 375-420, (2016).

[15] K. Koca, M.S. Genç., E. Bayır, F. K. Soğuksu, *Experimental study of the wind turbine airfoil with the local flexibility at different locations for more energy output,* Energy, **239**, 121887, (2022).

[16] M.S. Genç, Ü. Kaynak, G.D. Lock, *Flow over an Aerofoil without and with Leading Edge Slat at a Transitional Reynolds Number,* Proceedings of the Institution of Mechanical Engineers, Part G: Journal of Aerospace Engineering, **223**(3), 217-231, (2009).

[17] M.S. Genç, H. Demir, M. Özden, T.M. Bodur, *Experimental Analysis of Fluid-Structure Interaction in Flexible Wings at Low Reynolds Number Flows,* Aircraft Engineering and Aerospace Technology, **93**(6), 1060-1075, (2021).

[18] S. Keskin, M. Ayvazoğlu, M. Sincar, E. A. Sezer, H. H. Açıkel, M. S. Genç, "Effect of Airfoil Thickness on Flow Over the Cambered Airfoils,"in Proc. of the *2023 10th International Conference on Recent Advances in Air and Space Technologies (RAST), 07-09 June 2023 Istanbul, Turkiye, pp. 1-7.* Available: IEEE Xplore, https://ieeexplore.ieee.org/abstract/document/10197923.   [Accessed: 18 March 2024]. https://ieeexplore.ieee.org/abstract/document/10197923

[19] H. W. Emmons, *The laminar-turbulent transition in a boundary layer-Part I,* Journal of the Aeronautical Sciences, **18**(7), 490-498 (1951).

[20] J. Steelant, E. Dick, *Modelling of by-pass transition with conditioned Navier-Stokes equations and a k-epsilon model adapted for intermittency,* In Turbo Expo: Power for Land, Sea, and Air, American Society of Mechanical Engineers, 78835, (1994).

[21] Y.B. Suzen, G. Xiong, P.G., Huang, *Predictions of transitional flows in low-pressure turbines using intermittency transport equation,* AIAA journal, **40**(2), 254-266 (2002).

[22] F.R. Menter, R.B. Langtry, S.R. Likki, Y.B. Suzen, P.G. Huang, S. Völker, *A correlation-based transition model using local variables-part I: model formulation,* Journal of turbomachinery, **128**(3), 413-422 (2006).

[23] F.R. Menter, R.B. Langtry, S. Völker, *Transition modelling for general purpose CFD codes, Flow,* turbulence and combustion, **77**, 277-303, (2006).

[24] M. Julien, *Numerical investigations of separation-induced transition on high-lift low pressure turbine using RANS and LES methods.* Proceedings of the Institution of Mechanical Engineers, Part A: Journal of Power and Energy, **228**(8), 924-952, (2014).

To Cite This Article: M. Ayvazoglu, S. Keskin, R. Sahin, M. Sincar, E.A. Sezer, H.H. Acikel, M. Ozden, M.S. Genc, *Numerical and Experimental Investigation of Thickness Effect on the Cambered Airfoils at Low Reynolds Numbers*, Journal of Aeronautics and Space Technologies **17**(Special Issue), 116-134 (2024).

VITAE

Muhammer Ayvazoğlu received her B.Sc. degree in Energy Systems Engineering in Erciyes University, Türkiye. He is currently a MSc student in Erciyes University.

Sinem Keskin received her B.Sc. degree in Energy Systems Engineering from Faculty of Technology, Gazi University, Türkiye in 2018. She received her M.Sc. degree in Energy Systems Engineering from Faculty of Technology, Gazi University, Türkiye in 2023. She is currently a PhD student and working as a Research Assistant in Erciyes University.

Rumeysa Şahin received her B.Sc. degree in Energy Systems Engineering in Erciyes University, Türkiye. She is currently a MSc student in Erciyes University and working as a Research Assistant in Osmaniye Korkut Ata University.

Mehmet Sincar received her B.Sc. degree in Aerospace Engineering in Gaziantep University, Türkiye. He is currently a MSc student in Samsun University.

Eren Anıl SEZER received her B.Sc. degree in Energy Systems Engineering in Erciyes University, Türkiye. He is currently a MSc student in Erciyes University.

Dr. Halil Hakan AÇIKEL received her B.Sc. degree in Mechanical Engineering in Erciyes University, Türkiye. He received her M.Sc. and PhD. degree in Energy Systems Engineering in Erciyes University. He is currently an Assist. Prof. in Erciyes University.

Dr. Mustafa ÖZDEN received her B.Sc. degree in Energy Systems Engineering in Erciyes University, Türkiye. He received her M.Sc. and PhD. degree in Energy Systems Engineering in Erciyes University. He is currently a Postdoc Researcher at Clemson University.

Prof. Dr. M. Serdar GENÇ received her B.Sc. degree in Mechanical Engineering in Erciyes University, Türkiye. He received her M.Sc. and PhD. degree in Mechanical Engineering in Erciyes University. He is the head of Wind Engineering and Aerodynamics Research-WEAR Group.